Biophysical Chemistry 7 (1977) 15–32

THE HEMOLYTIC PLAQUE ASSAY: THEORY FOR FINITE LAYERS*

Byron GOLDSTEIN‡ and Alan S. PERELSON
Theoretical Division, University of California, Los Alamos Scientific Laboratory, Los Alamos, New Mexico 87545, USA

Received 26 October 1976

We extend the mathematical theory of hemolytic plaque growth to include plaques produced by cells secreting antibodies in layers of finite thickness. Previous theories have assumed that the layer was either two-dimensional or of infinite thickness. By using the method of images we derive an equation for the plaque radius as a function of time for layers of any thickness. We show that at short times and at long times the equation reduces to the appropriate infinite three-dimensional and two-dimensional limiting forms, and obtain expressions for estimating the range of times for which these limiting results are valid. For the liquid monolayer technique we obtain a new limiting result. The equation for the plaque radius is a transcendental equation which we solve numerically for a number of cases of interest. These results illustrate a variety of different features of plaque growth associated with the finite thickness of the layer. Experimental studies are usually carried out in layers whose thicknesses are not standardized. In the assays commonly used the thickness h can vary more than six hundred fold, i.e. 1×10^{-3} cm $\lesssim h \lesssim 6.5 \times 10^{-1}$ cm. Such variation in h will cause widely different kinetics of plaque growth. For typical plaque experiments of one hour duration the two-dimensional limit is valid when $h \lesssim 3 \times 10^{-3}$ cm while the infinite thickness limit is valid when $h \gtrsim 10^{-1}$ cm. For thicknesses in between these values the finite layer results must be used.

1. Introduction

The great diversity in the specificity of the cells and molecules of the immune system has presented major technical difficulties impeding the advance of experimental immunology. The recognition by Edelman that Bence–Jones proteins were a homogeneous population of immunoglobulin light chains secreted by a myeloma tumor made possible the determination of the primary structure of immunoglobulin [1]. Of similar importance was the development by Jerne and Nordin of a simple method of identifying those lymphocytes in a population which respond to a given antigen [2]. This technique, known as the *Jerne hemolytic plaque assay*, has allowed much information to be obtained about the dynamics of the immune response and the collaboration between various cell populations in augmenting or suppressing the response. Under appropriate circumstances the plaque assay can also be used to ascertain fundamental properties of antibody secreting cells, such as the number of antibodies secreted per unit time [3,4], the affinity [5], and possibly even the electrophoretic mobility [6] of the secreted antibodies.

In order to obtain quantitative information about antibody secreting cells a mathematical theory of plaque growth is necessary. DeLisi and Bell [7] have developed a theory for spherical plaque formation in agar which is infinite in extent in all three spatial dimensions. DeLisi [8] and Goldstein [9] have extended the theory to include plaques formed in monolayers of red blood cells. However, neither the infinite three-dimensional nor the infinite two-dimensional geometries correspond to the geometry of the actual assay system. It is the purpose of this communication to present a general theory of plaque growth valid in layers of finite thickness and to access the circumstances under which the simpler infinite two- and three-dimensional solutions are valid approximates to the actual solution.

* Work performed under the auspices of the U.S. Energy Research Development Administration.
‡ Permanent address: Department of Physics, Fairleigh Dickinson University, Teaneck, New Jersey 07666, USA.

In section 2 we discuss the experimental procedure followed in performing the hemolytic plaque assay with particular attention devoted to the physical dimensions of the various assay systems. Section 3 presents the mathematical theory of plaque growth. Here we restrict our attention to cases in which the interaction between antibody and antigenic sites on red blood cells is reversible and equilibrium controlled. Other cases can be treated by similar mathematical techniques (see appendix 2). In section 4 we discuss the qualitative behavior of our solutions, compare them to the previously determined infinite two- and three-dimensional approximations, and suggest the experimental circumstances under which each solution is valid. In section 5 we summarize our results and discuss their importance. A list of symbols is appended to the paper.

2. The assay

The hemolytic plaque technique as first introduced by Jerne and Nordin [2,10] permits the detection of lymphoid cells which produce antibodies against red blood cell (RBC) antigens[‡]. In the technique lymphoid cells, usually from the spleen of a mouse previously immunized with sheep RBC, are combined with antigen (sheep RBC) and nutrient medium in an agar layer. The layer is incubated at 37°C for one to two hours after which it is flooded with guinea pig complement. The complement causes the lysis of RBC that have sufficient numbers of antibodies bound on their surfaces. The lysed cells form clear areas in the agar, called *plaques*. Each plaque has at its center an antibody-forming cell (AFC) which secretes antibody. The diffusion of the secreted antibody radially outward from the AFC causes the formation of plaques which are initially spherically symmetric. Cell concentrations are chosen such that the plaques from different AFC do not overlap.

Humphrey [11] has estimated that one IgM molecule on a RBC surface is sufficient to bind complement but approximately 800 IgG molecules are needed for lysis to occur. Because IgM is so much more efficient at binding complement than IgG, this technique usually detects only IgM secreting cells.

Since its introduction the hemolytic plaque technique has undergone considerable modification and extension. (For a detailed description of these modifications as well as a complete list of references, see the recent review article by Jerne et al. [12].) For example, AFC which make antibodies against a wide variety of haptens and antigens can now be detected by using RBC with haptens or antigens covalently coupled to their surface [12–16]. AFC that secrete IgG can be made to produce plaques by using certain "indirect" techniques [17–19]. Substitutes for agar are now used [20] and liquid layer methods which use no support material are frequently employed [21–23]. Also microchamber techniques which use very thin layers to detect AFC are now in wide use [21,24–26].

In the plaque-in-agar method a petri dish is first coated with a layer of pure agar. A top agar layer containing AFC, RBC, spleen cells and nutrients is then poured over the bottom agar layer. Compiement can be added to the top agar layer at the initiation of the experiment or after the cells have incubated for an hour. In the plaque-in-agar experiments of Merchant and Peterson [26] the thickness of the top agar layer was approximately 0.15 cm. For these experiments the thickness of the bottom layer was not reported, but in general it ranges from 0.1–0.5 cm [10,27]. Thus for these experiments the total layer thickness $h \lesssim 0.65$ cm. In this technique plaque radii are of the order of 0.005 cm, but range up to 0.02 cm [2,26]. More recently the bottom layer has been dispensed with in favor of a single layer coated onto a slide.

In the liquid microchamber technique small chambers on microscope slides are filled with AFC, RBC, complement and culture medium. Since there is no support material the cells settle to the bottom and form a monolayer [22]. However, the height of the chamber is considerably larger than a single cell diameter. In the experiments of Merchant and Peterson the chamber thickness $h \approx 0.003$ cm, with plaque radii ranging between 0.002 cm and 0.04 cm [26], while in the liquid layer experiments of Cunningham and Szenberg, $h \approx 0.01$ cm [22] and the plaque radii ranged up to 0.035 cm [28].

Nossal et al. [25,29] modified an assay system first introduced by Ingraham and Bussard [20] that used carboxymethylcellulose (CMC) as a support material

[‡] Abbreviations: RBC, red blood cells; AFC, antibody forming cells; IgM, immunoglobin M; IgG, immunoglobin G.

and developed it into a monolayer technique. In their technique open layers 0.0012 cm thick of CMC containing AFC, RBC, complement and culture medium were made on coverslips and covered with paraffin oil to prevent evaporation. Average plaque radii were 0.006 cm but extended up to 0.01 cm [29].

As can be seen, there is wide variation in the thickness of the layers employed in the various plaque assays. In the experiments surveyed above, there is over a six hundred fold variation in layer thicknesses, i.e. $0.001 \text{ cm} \lesssim h \; 0.65$ cm. The kinetics of plaque growth is determined in part by the thickness of the layer. (In the plaque-in-agar technique when a bottom layer is employed, it is the total thickness of the bottom plus the top layer which must be considered, since antibodies can diffuse into either layer.) In order to correlate plaque size with various physical parameters such as the rate of antibody secretion by the AFC or the affinity of the antibody an accurate mathematical description of plaque growth is needed.

3. The theory

3.1. The limiting cases

The mathematical theory of the growth of hemolytic plaques has been developed for two limiting cases: the infinite three-dimensional case in which the gel is assumed to be infinite in all three spatial dimensions so that the diffusion of the secreted antibodies is unaffected by any boundaries; the two-dimensional case in which the layer is assumed to be infinite in extent but sufficiently thin that there is no variation in the antibody concentration in the direction perpendicular to the layer. In the infinite three-dimensional case the plaques are spherical, while in the two-dimensional case they are cylindrical. We first review the results for these cases since they will be important in obtaining and understanding the solution to the finite layer problem.

As an idealized model consider an AFC that secretes antibodies isotropically at a constant rate S. These antibodies are assumed to diffuse in a layer of thickness h with a constant diffusion coefficient D and to bind to sites on the surfaces of RBC. The RBC are taken to be distributed uniformly in the layer. Let $c(x, y, z, t)$ be the free antibody concentration, let $c_b(x, y, z, t)$ be the concentration of antibodies bound to RBC at (x, y, z) and let t be the secretion time, i.e. $t = T - T_0$, where T is the total time the AFC has been in the layer and T_0 is the time at which the AFC started to secrete antibody. At $t = 0$, $c = c_b = 0$.

For the infinite three-dimensional case ($h \to \infty$) the free antibody concentration obeys the following equation:

$$\partial c/\partial t = D\nabla^2 c - \partial c_b/\partial t + S\delta(r), \tag{1a}$$

with the boundary condition, $c(r, t) \to 0$, as $|r| \to \infty$. Here the AFC is treated as a point source situated at the origin, r is a three-dimensional position vector, pointing from the origin to the point with coordinates $r = (x, y, z)$, and $\delta(r)$ is the three-dimensional Dirac delta function [$\delta(r) = \delta(x)\delta(y)\delta(z)$]. The three terms on the right hand side of eq. (1a) represent changes in the free antibody concentration due to diffusion, binding to RBC, and, at the origin, production of antibodies.

For the two-dimensional case (h finite) the AFC is treated as a cylindrical source situated at the origin. The appropriate equation is then

$$\partial c/\partial t = D\nabla^2 c - \partial c_b/\partial t + (S/h)\delta(R), \tag{1b}$$

with the boundary condition $c(R, t) \to 0$ as $|R| \to \infty$ for all finite t. Here h is the thickness of the layer, R the two-dimensional position vector and $\delta(R)$ the two-dimensional Dirac delta function [$\delta(R) = \delta(x)\delta(y)$]. The factor h is included in the source term so that when integrated over any volume that includes the entire source, S antibodies are secreted per second, i.e.

$$\int_0^h \iiint (S/h)\delta(R)\,dx\,dy\,dz = S.$$

To proceed, an equation for the rate of change in the bound antibody concentration is needed. We shall assume that the binding of antibody to an antigenic determinant on the RBC surface follows the law of mass action

$$\partial c_b/\partial t = \upsilon k_f c\rho - k_r c_b, \tag{2}$$

where k_f and k_r are the rate constants describing the binding and the dissociation of an antibody combining site with the cell surface, υ is the antibody valence (10 for IgM) and ρ is the concentration of free antigenic determinants.

There is indirect experimental evidence that for

direct plaques formed in layers which contain RBC antigens or sparsely haptenated RBC (10^5 hapten/RBC or less), the free and bound antibody concentrations are in local equilibrium [6,8]. If we assume local equilibrium [i.e. $\partial c_b/\partial t = 0$ in eq. (2)] then

$$c_b = \upsilon K c \rho, \tag{3}$$

where $K = k_f/k_r$ is the affinity of a single antibody combining site for a single RBC antigenic determinant (epitope).

For local equilibrium to obtain, the antibodies must rapidly go on and off the RBC surfaces. This implies that the binding is by single site attachment [30]. (When antibodies bind multivalently the attachments are very long-lived and local equilibrium is not a good assumption [31].) With single site binding the free antibody concentration, which is due to the secretion of antibodies by a single AFC, is never high enough for a large fraction of the RBC sites to be bound at measurable distances from the AFC [3]. If ρ_0 is the total concentration of the antigenic sites, i.e. $\rho_0 \equiv e\rho_{RBC}$, where e is the number of epitopes on a single RBC, and ρ_{RBC} is the RBC concentration, then $\rho \approx \rho_0$. When this condition holds eq. (2) becomes

$$c_b = \upsilon K \rho_0 c. \tag{4}$$

The constraints of local equilibrium, single site attachment and $\rho \approx \rho_0$ may be somewhat restrictive. For our purposes we shall only require the validity of eq. (4) and not the full implications of these conditions. For example, at long times, models of multisite attachment which utilize sequential binding reactions and $\rho \approx \rho_0$ may also give rise to eq. (4) [31].

When eq. (4) is substituted into eq. (1a) or (1b) a diffusion equation is obtained,

$$\frac{1}{D^*}\frac{\partial c}{\partial t} = \nabla^2 c + \frac{S}{D}\delta(r), \qquad \text{three-dimensional;} \tag{5a}$$

$$\frac{1}{D^*}\frac{\partial c}{\partial t} = \nabla^2 c + \frac{S}{hD}\delta(R), \qquad \text{two-dimensional,} \tag{5b}$$

where D^* is the hindered diffusion coefficient

$$D^* = D/(1 + \upsilon K \rho_0). \tag{6}$$

The solutions to eqs. (5a) and (5b) are [8]

$$c(r, t) = (S/4\pi Dr)\,\mathrm{erfc}[(r^2/4D^*t)^{1/2}], \qquad \text{three-dimensional;} \tag{7a}$$

$$c(R, t) = (S/4\pi Dh)E_1(R^2/4D^*t), \qquad \text{two-dimensional,} \tag{7b}$$

where erfc (·) is the complementary error function, and E_1(·) is the exponential integral of order one.

To define the plaque radius we assume that at the plaque radius there are N antibodies bound per RBC (for IgM Jerne has estimated that N is between 1 and 10 [12]). With this definition and eq. (4),

$$N = c_b/\rho_{RBC} = \upsilon K e c. \tag{8}$$

Since eq. (8) is only satisfied at the plaque radius, the following equations can be obtained for the two- and three-dimensional plaque radii, r_p and R_p, respectively,

$$4\pi DN/\upsilon KeS = (1/r_p)\,\mathrm{erfc}[(r_p^2/4D^*t)^{1/2}], \qquad \text{three-dimensional;} \tag{9a}$$

$$4\pi DhN/\upsilon KeS = E_1(R_p^2/4D^*t), \qquad \text{two-dimensional.} \tag{9b}$$

The left hand side of eq. (9b) is a constant which implies that the argument of E_1(·) must be constant. Thus, the theory predicts that for very thin layers R_p^2/t = constant. This has been observed [20,25,29]. In three dimensions antibodies can diffuse over a larger volume than in two dimensions and hence we expect r_p^2 to grow more slowly than the first power of t. If this is so, then as t becomes very large, r_p^2/t goes to zero, erfc $(r_p^2/4D^*t)$ goes to one, and the plaque radius approaches a constant: $r_p(t \to \infty) = \upsilon KeS/4\pi DN$. This result is indeed true and can be obtained in a rigorous fashion by setting $\partial c/\partial t = 0$ in eq. (5a), solving for c in the steady state, and substituting into eq. (8).

In the assay systems used in the laboratory h is rarely greater than 0.6 cm and usually is considerably smaller. One expects the three-dimensional approximation to be valid if the plaque diameters are small compared to h. However, even if this is the case some AFC will be near the top or bottom of the layer causing the effects of the boundary to be felt. For layers with $h \approx 0.01$ cm the plaque radii are expected to be of the same order of magnitude as h and neither the two-dimensional nor three-dimensional approximations will be valid for a wide range of times. No matter what the thickness of the finite layer, at long

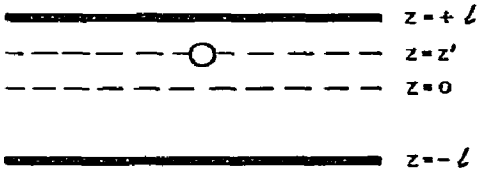

Fig. 1. An antibody forming cell (○) a distance z' above the center of a layer. The thickness of the layer equals $2l$.

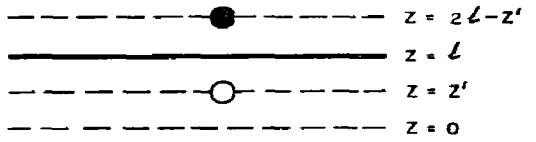

Fig. 2. An antibody forming cell (○) in front of a single boundare plane. The image source (●) at $z = 2l - z'$, and the antibody forming cell at $z = z'$ are equidistant from the plane at $z = l$.

enough times the two-dimensional result will eventually hold, provided of course the AFC secretes antibodies at a constant rate for the entire experiment. For a given layer thickness it is clearly of interest to know how long the three-dimensional approximation holds and at what time the two-dimensional approximation becomes valid. To answer such questions, and to obtain a plaque theory valid for all times, we now consider plaque formation in finite layers.

3.2. The finite layer

We again consider an AFC in a layer of infinite extent and finite thickness h, but now we do not ignore the diffusion of antibody perpendicular to the layer. The layer can be thought of as being bounded by two infinite planes through which antibodies can not pass. We set up a coordinate system such that the planes are at $z = +l$ and $z = -l$, $h = 2l$ (see fig. 1), and the AFC is off center at the point $(0, 0, z')$, $-l \leqslant z' \leqslant l$. The problem is to solve the following equation for $t \geqslant 0$,

$$(1/D^*)\,\partial c/\partial t = \nabla^2 c + (S/D)\delta(x)\delta(y)\delta(z-z'), \qquad (10)$$

subject to the boundary conditions that at $z = \pm l$, the antibody flux perpendicular to the boundaries vanish, i.e. $\partial c/\partial z = 0$ at $z = \pm l$ and $c(x, y, z, t) \to 0$ as $x, y \to \infty$ for all finite t. For $t \leqslant 0$, $c = 0$.

We solve this problem by the method of images, a technique commonly used in electrostatics [32]. We extend the medium to $z = \pm\infty$ and replace the boundary conditions by fictitious (image) sources placed outside the boundaries, whose positions and magnitudes are chosen in such a way that $\partial c/\partial z = 0$ at $z = \pm l$.

Rather than solve eq. (10) directly we first solve for $c' = \partial c/\partial t$ and then integrate c' over time to obtain c.

$$c(x, y, z, t) = \int_0^t c'(x, y, z, \tau)\,\mathrm{d}\tau. \qquad (11)$$

By differentiating eq. (10) with respect to time it can be seen that c' obeys the equation‡

$$(1/D^*)\,\partial c'/\partial t = \nabla^2 c' + (S/D)\delta(t)\delta(x)\delta(y)\delta(z-z'), \qquad (12)$$

with $\partial c'/\partial z = 0$ at $z = \pm l$. Eq. (12) has been solved for the same geometry but a different boundary condition, $c' = 0$ at $z = \pm l$, by Carslaw and Jaeger [33]. We use the same techniques as outlined by Carslaw and Jaeger to solve our problem.

The solution to eq. (12) for the infinite three-dimensional case is

$$c'(r, t) = (SD^*/8D)(\pi D^* t)^{-3/2} \exp[-(r')^2/4D^*t], \qquad (13)$$

where $(r')^2 = x^2 + y^2 + (z-z')^2$. If eq. (13) is integrated from 0 to t, eq. (7a) is reobtained.

The solution to eq. (12) if just one boundary is present at $z = l$ with $z' < l$ (see fig. 2) is,

$$c'(R, z, t) = (SD^*/8D)(\pi D^* t)^{-3/2} \exp(-R^2/4D^*t) \times \{\exp[-(z-z')^2/4D^*t] + \exp[-(z+z'-2l)^2/4D^*t]\}, \qquad (14)$$

where $R^2 = x^2 + y^2$. This is because only one image source, at $z = 2l - z'$, is needed to satisfy the boundary condition at $z = l$.

When two boundary planes are present an infinite number of image sources are needed since every time

‡ c' is the Green's function for this problem. Eq. (12) follows from eq. (10) by noting that the right hand side of eq. (10) can be written for all t as $SH(t)\delta(x)\delta(y)\delta(z-z')/D$ where $H(t)$ is the Heaviside function: $H(t) = 1$ for $t \geqslant 0$ and $H(t) = 0$ for $t < 0$. This function has the property that $\mathrm{d}H(t)/\mathrm{d}t = \delta(t)$.

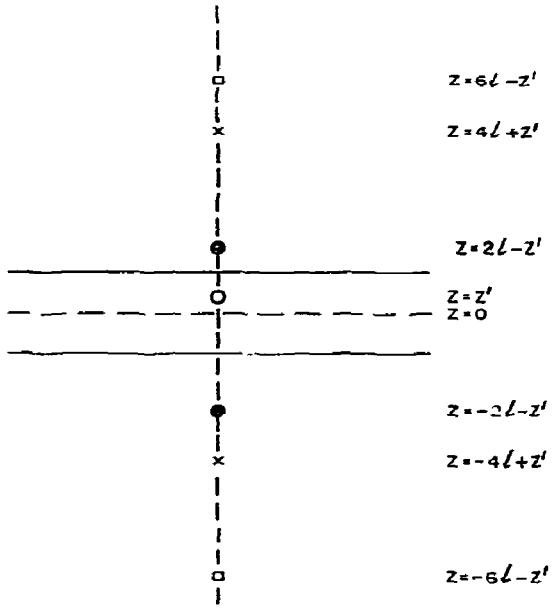

Fig. 3. An antibody forming cell (○) a distance z' above the center of a layer. The boundary planes of the layer are at $z = \pm l$. The first six image sources are shown. • is an image of ○, × an image of •, and □ an image of ×.

an image source is introduced to satisfy the boundary condition at one plane, it causes the boundary condition to no longer be satisfied at the other plane. In fig. 3 the positions of the required image sources are shown. From this figure and eq. (13) it is straightforward to write down the solution to eq. (12),

$$c'(R,z,t) = (SD^*/8D)(\pi D^* t)^{-3/2}\exp(-R^2/4D^*t) \times \{\exp[-(z-z')^2/4D^*t] + \exp[-(z+z'+2l)^2/4D^*t] + \exp[-(z+z'-2l)^2/4D^*t] + \exp[-(z-z'+4l)^2/4D^*t] + \exp[-(z-z'-4l)^2/4D^*t] + \exp[-(z+z'+6l)^2/4D^*t] + \exp[-(z+z'-6l)^2/4D^*t] \ldots\}, \quad (15)$$

which can be rewritten in the following form:

$$c'(R,z,t) = (SD^*/8D)(\pi D^* t)^{-3/2}\exp(-R^2/4D^*t) \times \left[\sum_{n=-\infty}^{n=\infty} \exp\{-[z+z'+(2n-1)2l]^2/4D^*t\} + \sum_{n=-\infty}^{\infty} \exp[-(z-z'+4nl)^2/4D^*t]\right]. \quad (16)$$

To obtain an expression for the free antibody concentration we substitute eq. (16) into eq. (11), the result being that

$$c(R,z,t) = (S/4\pi Dh)\sigma_3, \quad \text{3-dim. expansion,} \quad (17)$$

where

$$\sigma_3 = h\sum_{n=-\infty}^{\infty}\left[\frac{\operatorname{erfc}\beta_n^{1/2}}{r_n} + \frac{\operatorname{erfc}B_n^{1/2}}{L_n}\right], \quad (18a)$$

$$\beta_n = r_n^2/4D^*t, \quad (18b)$$

$$r_n^2 = R^2 + (z-z'+4nl)^2, \quad (18c)$$

$$B_n = L_n^2/4D^*t, \quad (18d)$$

$$L_n^2 = R^2 + (z+z'-2l+4nl)^2. \quad (18e)$$

Note that for $n = 0$ the first term in eq. (18a) when substituted into eq. (17) is just the infinite three-dimensional result, where the source is at $(0,0,z')$. When $z' = 0$, σ_3 reduces to

$$\sigma_3 = (h/r)\operatorname{erfc}[(r^2/4D^*t)^{1/2}] + h\sum_{\substack{n=-\infty \\ n\neq 0}}^{\infty}\operatorname{erfc}[(d_n^2/4D^*t)^{1/2}]/d_n, \quad (19)$$

where $d_n^2 = R^2 + (z+2nl)^2$. The first term on the right corresponds to the three-dimensional solution [eq. (7a)].

Although the sum in eq. (17) converges for all finite values of the parameters, only for short times will it converge rapidly. We therefore obtain another expression for $c(R,z,t)$ which converges rapidly for long times. To do this we use the following identity (see p. 275 of ref. [33]):

$$\sum_{n=-\infty}^{\infty}\exp[-(z+2nl)^2/4D^*t] = [(\pi D^*t)^{1/2}/l] \times \left[1 + 2\sum_{n=1}^{\infty}\cos(n\pi z/l)\exp(-n^2\pi^2 D^*t/l^2)\right].$$

With this identity, eq. (16) becomes

$$c'(R,z,t) = (S/8\pi Dtl)\exp(-R^2/4D^*t)$$

$$\times \left[1 + \sum_{n=1}^{\infty} \{(-1)^n \cos[n\pi(z+z')/2l] + \cos[n\pi(z-z')/2l]\} \exp(-n^2\pi^2 D^* t/4l^2)\right]. \quad (20)$$

When this expression for $c'(R, z, t)$ is integrated from 0 to t, one obtains

$$c(R, z, t) = (S/4\pi Dh)\sigma_2, \quad \text{2-dim. expansion,} \quad (21)$$

where

$$\sigma_2 = E_1(R^2/4D^*t) + \sum_{n=1}^{\infty} \{(-1)^n \cos[n\pi(z+z')/2l] + \cos[n\pi(z-z')/2l]\} I_n. \quad (22)$$

I_n is the following integral (its properties are discussed in ref. [6]):

$$I_n = \int_0^t (t')^{-1} \exp[-(R^2/4D^*t' + n^2\pi^2 D^* t'/4l^2)]\, dt'. \quad (23)$$

Note that the first term in eq. (22) when substituted into eq. (21) gives the two-dimensional result [eq. (7b)].

We now have two expressions for $c(R, z, t)$, one which we expect to converge rapidly for short times and one which we expect to converge rapidly for long times. We are interested in how plaque radii grow with time which means we must solve eq. (8). The two equivalent equations for the plaque radius which we study in the next section are,

$$4\pi DhN/\upsilon KeS = \sigma_3(R, z, t), \quad \text{3-dim. expansion;} \quad (24a)$$

$$4\pi DhN/\upsilon KeS = \sigma_2(R, z, t), \quad \text{2-dim. expansion,} \quad (24b)$$

where σ_3 and σ_2 are given by eqs. (18a) and (22), respectively.

4. Results

For an AFC near the center of a gel, at short times, the plaque will be spherical and grow as if it were in an infinite three-dimensional medium, while at long times the plaque will be cylindrical and grow as if the diffusion were planar. To visualize this one can think of the plaque as a leaky baloon being blown up by having air enter it at a constant rate[#]. Initially the balloon will be spherical, then it will come in contact with the boundary planes and deform. As time goes on the top and bottom will flatten and the balloon's shape will become more and more cylindrical.

4.1. Times for which the two-dimensional solution is valid

To see when the two-dimensional solution applies consider the sum σ_2 given by eq. (22). When

$$E_1(R^2/4D^*t) \gg \sum_{n=1}^{\infty} \{(-1)^n \cos[n\pi(z+z')/2l] + \cos[n\pi(z-z')/2l]\} I_n, \quad (25)$$

σ_2 can be approximated by $E_1(R^2/4D^*t)$ giving the two-dimensional result, eq. (7b). I_n has the property that $K_0(\gamma_n R) \geqslant I_n$, where $\gamma_n = \pi n/h$ and $K_0(\cdot)$ is the modified Bessel function of order zero [6]. We can overestimate the right hand side of eq. (25) by replacing I_n with $K_0(\gamma_n R)$ and the two cosine terms in brackets by +2. Thus when

$$E_1(R^2/4D^*t) \gg 2\sum_{n=1}^{\infty} K_0(\gamma_n R), \quad (26)$$

the two-dimensional result holds and the plaque radius is given by [see eq. (9b)]

$$\theta = E_1(\beta), \quad (27)$$

where $\theta = 4\pi DhN/\upsilon KeS$ and $\beta = R_p^2/4D^*t$.

$K_0(\gamma_n R)$ decreases monotonically with increasing $\gamma_n R$ and hence with increasing values of n. In fact, for large values of its argument $K_0(\cdot)$ decreases exponentially [34]. Thus to obtain an order of magnitude estimate for the time at which eq. (26) holds at the plaque radius we replace the sum by its first term, $K_0(\gamma_1 R_p)$. For some value of $\gamma_1 R_p$ which we call m, $\theta \gg 2K_0(m)$ for all $\gamma_1 R_p \geqslant m$ and the two-dimensional solution will be valid. Since $R_p = (4D^*t\beta)^{1/2}$, where β is a constant related to θ through eq. (27), the inequality $\gamma_1 R_p \geqslant m$ can be rewritten to yield

$$t \geqslant t_2 \equiv m^2 h^2/4\pi^2 D^* \beta, \quad (28)$$

[#] We assume that the balloon is leaky since antibodies can diffuse beyond the plaque radius. This analogy is still not perfect and should not be relied on heavily. However, it does provide insight into the effects of geometry on the dynamics of plaque growth.

Table 1 [a]

h (10^{-3} cm)	θ	β	m	t_2 (s)
1.0	0.5	5.5×10^{-1}	5.3	8
2.0	1.0	2.6×10^{-1}	4.7	51
3.0	1.5	1.4×10^{-1}	4.3	177
4.0	2.0	8.2×10^{-2}	4.1	489
5.0	2.5	4.8×10^{-2}	3.9	1180
10.0	5.0	3.8×10^{-3}	3.3	42700

[a] t_2 is the estimated time, beyond which the two-dimensional solution is valid. m was chosen such that $\theta/200 = K_0(m)$ in order that the condition $\theta \gg 2K_0(m)$ be met. β satisfies the equation $\theta = E_1(\beta)$ and its value was obtained from computer generated tables for the exponential integral of order one. The value of θ/h used is a typical value [6], which can be obtained from the following set of parameters: $N = 2$, $D^* \approx D = 1.7 \times 10^{-7}$ cm^2/s, $K = 5 \times 10^4$ M^{-1}, $v = 10$, $e = 10^4$ sites/RBC and $S = 10^3$ Ab/s.

where t_2 is a lower bound on the time necessary for two-dimensional plaque growth.

The dependence of t_2 on h is somewhat greater than the second power (h^2) because of the dependency of m^2/β on h. This can be seen from table 1 where we list values of t_2 for different values of h. In order to evaluate m we assumed θ was 100 times greater than $2K_0(m)$.

t_2 depends on the properties of the AFC as well as on the thickness of the layer. As θ decreases for fixed h (which corresponds to a stronger AFC in the sense of higher emission rates or affinities) m^2/β decreases and t_2 goes down. The reasonableness of this result can be seen by the following argument: the more antibodies secreted per second the more rapidly antibodies diffuse to the boundary (due to increases in the concentration gradient) and the more rapidly the variation in the free antibody concentration in the z-direction disappears. Values of t_2 for different values of θ are listed in table 2. Weak antibody secreters correspond to large values of θ/h and therefore, for fixed h, t_2 increases with increasing θ/h. The θ/h values in table 2 were chosen to reproduce the experimentally observed range of plaque radii. For $t \approx 60$ min, the duration of a typical plaque experiment, the two-dimensional limit will be valid when $h \lesssim 3 \times 10^{-3}$ cm for all AFC except the very weak secreters (when $h = 3 \times 10^{-3}$ cm and $\theta/h = 2000$ cm^{-1}, $t_2 = 143$ min). For very strong secreters h may be as large as 5×10^{-3} cm before the two-dimensional limit breaks down (when $h = 5 \times 10^{-3}$ cm and $\theta/h = 500$ cm^{-1}, $t_2 = 19.7$ min).

Table 2 [a]

h (10^{-3} cm)	θ/h (cm^{-1})				
	100	500	1000	1500	2000
1	0.08	0.13	0.21	0.33	0.51
2	0.4	0.8	2.0	7.9	20.4
3	0.9	3.0	10.6	38.6	143.2
4	1.9	8.1	48.7	254.6	1758.7
5	3.2	19.7	177.9	1684.3	17407.4

[a] t_2 in min. Each column corresponds to a particular value θ/h. The θ/h values were chosen to reproduce the experimentally observed range of plaque radii, i.e. for $t = 1$ h, $h = 3 \times 10^{-3}$ cm and $\theta/h = 100$ cm^{-1}, 500 cm^{-1}, 1000 cm^{-1}, 1500 cm^{-1} and 2000 cm^{-1}, respectively, $R_p = 448\ \mu$, 185 μ, 84 μ, 39 μ and 19 μ, respectively.

4.2. Times for which the three-dimensional solution is valid

To see when the inifinite three-dimensional result holds we consider the sum σ_3 given by eq. (18a). The $n = 0$ terms correspond to the source and the nearest image source. Other terms correspond to the contribution of more distant image sources. The infinite three-dimensional result will hold when the contribution of the actual source is much greater than that of its images. Since the nearest image source contributes the largest correction term we can get an order of magnitude estimate of the time span over which the infinite three-dimensional solution is a valid approximation by finding the time for which the contribution of the source is much greater than that of the nearest image source, i.e.

$$\operatorname{erfc}(\beta_0^{1/2})/r_0 \gg \operatorname{erfc}(B_0^{1/2})/L_0, \tag{29}$$

where $L_0 = [R^2 + (z+z'-2l)^2]^{1/2}$ and $B_0 = L_0^2/4D^*t$. Satisfaction of this inequality provides a necessary condition for the validity of the three-dimensional solution. We shall show that if the three-dimensional solution is valid then t must be less than some particular value t_3. This will imply that for $t > t_3$ the three-dimensional solution is not valid.

The right hand term in eq. (29) is largest when L_0

takes on its smallest value. This occurs along the z-axis where $R = 0$. Further, since we wish to know whether this inequality is satisfied at the plaque boundary, we choose $z = z' + r_p$, where r_p is the plaque radius measured along the z-axis. (Here we are assuming that z' is positive, i.e. that the AFC is in the upper half of the gel. If z' is negative we choose $z = z' - r_p$. When the three-dimensional solution holds, the plaque will be spherical and r_p will be the true plaque radius.) Thus in eq. (29) we replace L_0 by $2(l-z') - r_p$ which we write as $(1-f)h^*$, where $h^* = 2(l-z')$ is the distance between the source and its nearest image source, and $f = r_p/h^*$. Since the plaque radius must be smaller than the distance between the AFC and the top of the layer, $r_p \leqslant l - z'$ and f must lie between 0 and 0.5.

Substituting this value of L_0 into eq. (29) one finds

$$\operatorname{erfc}(\beta_0^{1/2})/r_0 \gg \operatorname{erfc}[(1-f)(B_0^*)^{1/2}]/(1-f)h^*, \qquad (30)$$

where $B_0^* \equiv (h^*)^2/4D^*t$. For times at which eq. (30) is valid, the three-dimensional solution is a good approximation and $4\pi DN/\upsilon KeS = \operatorname{erfc}(\beta_0^{1/2})/r_0$. Defining $\theta^* = 4\pi Dh^*N/\upsilon KeS$ eq. (30) becomes

$$(1-f)\theta^* \gg \operatorname{erfc}[(1-f)(B_0^*)^{1/2}]. \qquad (31)$$

Choosing a positive number q such that $(1-f)\theta^* \gg \operatorname{erfc}(q)$, and noting that erfc (·) is a monotonicly decreasing function one finds that eq. (31) is valid if $(1-f)(B_0^*)^{1/2} \geqslant q$, or equivalently, if

$$t \leqslant (1-f)^2(h^*)^2/4D^*q^2. \qquad (32)$$

Since $0 \leqslant f \leqslant 0.5$ and $f = 0.5$ only when the plaque radius hits the boundary, one would expect f to be small when the inifinite three-dimensional solution breaks down. Thus, we can replace eq. (32) by[‡]

$$t \leqslant t_3 \equiv (h^*)^2/4D^*q^2. \qquad (33)$$

In table 3 we obtain numerical values for t_3 for various values of h^* by choosing q such that $\operatorname{erfc}(q) = 0.01\theta^*$. Since $\operatorname{erfc}(q) \leqslant 1$ for all q, if $\theta \geqslant 100$, q is not defined and eq. (33) cannot be used to estimate t_3. In deriving eq. (33) only the source and its nearest image was considered (the $n = 0$ term in σ_3). When θ becomes large σ_3 converges slowly except at very short times. To derive an expression for t_3 which is valid for all θ the contributions from image sources more distant than the nearest must be taken into account. This is done in appendix 1. However, for $\theta \lesssim 50$ our numerical studies show eq. (33) is quite adequate. (For example, for an AFC at the center of a layer with $h = 0.05$ cm, $D = 1.7 \times 10^{-7}$ cm^2/s and $\theta = 25$, at $t = t_3$ the exact and infinite three-dimensional solution for the plaque radius in the $z = 0$ plane differ by 2%. With the same parameters and $\theta = 50$ the difference is 3%.)

Table 3 [a]

h^* (10^{-3} cm)	θ^*	q	t_3 (s)
2.0	1.0	1.83	1.8
3.0	1.5	1.72	4.5
4.0	2.0	1.64	8.8
5.0	2.5	1.59	14.5
10.0	5.0	1.39	76.1
50.0	25.0	0.82	5467.7

a) A necessary condition for the inifinite three-dimensional solution to be valid is $t \leqslant t_3$. q was chosen such that $\theta/100 = \operatorname{erfc}(q)$ in order that the condition $\theta \gg \operatorname{erfc}(q)$ be met. The same value of θ/h and D^* was used as in table 1, i.e. $\theta/h = 500$ cm^{-1} and $D^* \approx D = 1.7 \times 10^{-7}$ cm^2/s.

The three-dimensional result will first break down for the strongest secreters. When $\theta/h = 5.14$ cm^{-1} and $h = 10^{-1}$ cm, $t_3 = 1.04$ h. This θ/h value corresponds to a very strong secreter. It can be obtained from the following set of parameters: $N = 2$, $D^* \approx D = 1.7 \times 10^{-7}$ cm^2/s, $K = 10^5$ M^{-1}, $\upsilon = 10$, $e = 10^5$ sites/RBC and $S = 5 \times 10^3$ Ab/s. The experimentally observed θ/h values are usually larger than this. Thus, we expect the infinite three-dimensional limit to hold for $h \gtrsim 10^{-1}$ cm.

4.3. Numerical studies

Although we have obtained expressions for the dynamics of plaque growth in finite layers, the resulting equations [eqs. (24)] are implicit. Since we know of

[‡] A more rigorous estimate can be obtained by underestimating the right hand side of eq. (32). This can be done by overestimating f and q. In terms of f the infinite three-dimensional solution, eq. (9a), can be written as $f\theta^* = \operatorname{erfc}(fB_0)$. Since $\operatorname{erfc}(x) < 1$ for all x, $f > 1/\theta^*$. This inequality only holds for $\theta^* \geqslant 2$ since $f \leqslant 0.5$ (at $f = 0.5$ the plaque radius has reached the boundary and eq. (9a) can no longer hold). Thus one can take $f = 0.5$ for $\theta^* \leqslant 2$ and $f = 1/\theta^*$ for $\theta^* \geqslant 2$. For large values of θ^* estimates obtained this way approach those given by eq. (33).

no analytical procedure for obtaining the plaque radius as an explicit function of time we have solved eqs. (24) numerically. An algorithm developed by Dekker [35] for finding the zeroes of a real valued function was used to solve $\theta - \sigma_i = 0$, $i = 2$ or 3, for the plaque radius. The sum σ_3 which runs from $-\infty$ to ∞, was broken up into the $n = 0$ term, plus two sums which ran from 1 to ∞. These latter two sums, both of which were convergent, were truncated when the next term in the sum was less than 10^{-6} the value of sum. A similar convergence criterion was used for σ_2. However in order to exclude zero terms generated by the vanishing of the cosine terms, only the value of I_n was compared to that of the sum. The integrals I_n were evaluated by an adaptive seven-point Newton Cotes formula. Since the integrand had a very sharp maximum which could be missed by a mistaken choice of step size, the integration region was divided into sections such that the maximum occurred at the boundary between two sections.

We now report the results we obtained by solving eqs. (24) numerically. For liquid chambers we took $D^* \approx D = 1.7 \times 10^{-7}$ cm^2/s, the experimentally determined $D_{20,w}$ value for IgM [36,37]. In gel, D for IgM will vary depending on the gel composition. For our numerical work we took $D = 8 \times 10^{-8}$ cm^2/s for layers containing support material.

4.3.1. Thin agar layer

In fig. 4a the first 15 min of plaque growth is shown for an AFC at the center ($z' = 0$) of a thin agar layer ($h = 6.3 \times 10^{-3}$ cm). Eq. (33) predicts that for $t \lesssim 42$ s the infinite three-dimensional result will hold. One can see the curve for the infinite three-dimensional case does in fact hold for these times and begins to deviate from the exact solution for $t \approx 50$ s. Curves for the plaque radius at the top $z = l$, at $z = l/2$, and in the plane of the AFC ($z = 0$) are shown. At short times there is a large difference between the plaque radii measured in the $z = 0$ and $z = l$ planes. As t increases and the plaque becomes cylindrical this dispersion in the radii goes to zero (see fig. 4b). Eq.

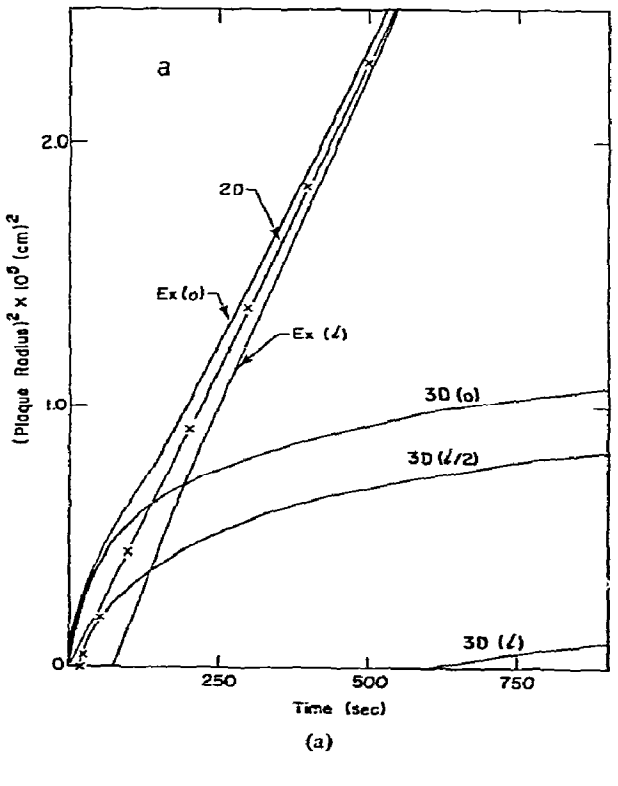

(a)

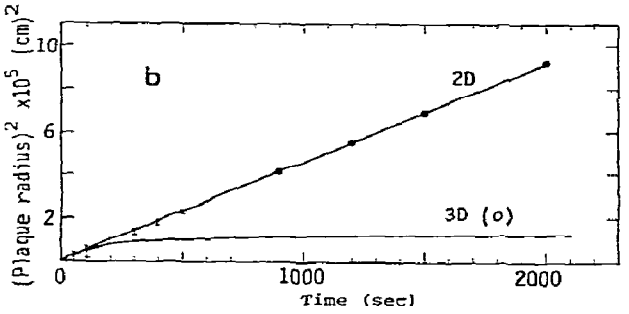

(b)

Fig. 4. (a) The plaque radius squared as a function of time for an AFC in the center of a layer ($z = 0$) of thickness $h = 6.3 \times 10^{-3}$ cm. For all curves $\theta = 1.5$ and $D = 8.0 \times 10^{-8}$ cm^2/s. The exact results for the plaque radius measured in the $z = 0$ and $z = l$ plane are given by curves Ex(0) and Ex(l). The X's are the exact values for the plaque radius measured in the $z = l/2$ plane. Shown also is the two-dimensional limit (2D) and the infinite three-dimensional limit. The three curves labeled 3D(0), 3D(l/2) and 3D(l), correspond to the plaque radii measured in the $z = 0$, $l/2$ and l planes, i.e. the radii of circles which are the intersections of those planes with a sphere whose radius corresponds to the infinite three-dimensional limit. (b) The same system as in (a). The points correspond to the exact solution. The top and bottom of the error bars correspond to the plaque measured in the $z = 0$ and $z = l$ planes respectively. Shown also are the curves for the two- (2D) and infinite three- (3D) dimensional limits. For the infinite three-dimensional limit the plaque is measured in the $z = 0$ plane.

(28) predicts that the two-dimensional result will hold for $t \geq 1680$ s. For $t = 1000$ s, $R_p = 6.80 \times 10^{-3}$ cm, 6.79×10^{-3} cm and 6.78×10^{-3} cm for $z = 0, l/2$ and l respectively. The two-dimensional limit predicts $R_p = 6.79 \times 10^{-3}$ cm. For this thin layer, even by 400 s, the two-dimensional result is within 2% of the actual solution at any point in the layer.

There are some additional noteworthy features of fig. 4a. First, at $z = l$ the plaque radius is essentially zero until $t \approx 80$ s (at 75 s the plaque radius at $z = l$ is computed to be 1.9×10^{-10} cm). At $z = l/2$ the radius is negligible until $t \approx 20$ s. These delays in the growth of the plaque reflect the finite time it takes a molecule to diffuse from the AFC at $z = 0$ to RBC at $z = l/2$ and $z = l$. Using the mean square distance a molecule diffuses in an infinite three-dimensional media, from a continuous source*, $\langle r^2 \rangle = 3Dt$, one finds that the time to diffuse to $z = l$ is 26 s. However, since enough molecules must diffuse so that at equilibrium N are bound to each RBC it is not surprising that the plaque radius is zero until a time greater than 26 s. Second, at the top of the layer ($z = l$) $R_p^2/t \approx$ constant for almost all times after the plaque appears. This may reflect the fact that by the time the plaque forms on the top layer there is very little variation of the antibody concentration in the z-direction. Third, at $z = l/2$ the plaque radius grows at a rate very close to that predicted by the two-dimensional solution for $t \geq 50$ s. The best agreement with the two-dimensional solution should be obtained somewhere between the AFC and the top of the layer. In the $z = 0$ plane the true plaque initially grows faster than that of a plaque produced by a source that is spread along a line of length h (a cylindrical emitter). At the top of the layer the true plaque initially grows more slowly than the cylindrical emitter primarily because of the delay involved in the antibodies reaching the top surface. For the case under study the plaque very quickly takes on the two-dimensional limiting behavior in the $z = l/2$ plane.

For plaque experiments performed in thin layers a plot of R_p^2 versus T has been found to yield a straight line with intercept T_0 at $R_p^2 = 0$ [20,25,28]. If there were no time lags present, and if the layer were sufficiently thin that the two-dimensional solution [eq. (9b)] held for the entire experiment, one would expect the R_p^2 versus T curve to go through the origin. The fact that $T_0 \neq 0$ leads one to believe that substantial time delays are present in the assay system. The value of the lag time, T_0, is probably due to the sum of many effects: (a) the AFC do not start secreting antibodies immediately after being placed in the layer, (b) once complement is fixed lysis does not occur instantaneously, (c) diffusional lags and (d) deviations from two-dimensional behavior. The importance of (c) and (d) will depend on the thickness of the layer and where in the layer the plaque radius is measured. Notice from fig. 4a that if the plaque radius is measured at the top surface, $z = l$, the diffusional lag and deviation from two-dimensional behavior give a positive contribution to T_0. However, if the plaque radius is measured at the level of the AFC, $z = 0$, a straight line fit to the data will yield a negative intercept (contribution to T_0). This apparent negative lag is due to the initial deviation from ideal two-dimensional growth in which R_p^2 at $z = 0$ grows faster than T.

4.3.2. Thick agar layer

If the AFC used to generate the plaque in fig. 4, which had $\theta/h \approx 238$, was placed in a thick gel ($h = 0.16$) of the same composition then $\theta \approx 38$. For such a cell in a thick gel the plaque radius obtained from the solution to the exact equation (9a) and the infinite three-dimensional result differ by less than 0.01% for $t \leq 8$ h as shown in fig. 5. Indeed eq. (33) predicts that the infinite three-dimensional result will hold for $t \lesssim 58$ h. Notice that the plaque exhibits quite different behavior in the thick and thin gels even though the AFC is identical. For the thin gel within a short time R_p^2/t approaches a constant (two-dimensional limit) while for the thick gel R_p appears to approach a constant (infinite three-dimensional limit). One should also notice that since R_p remains essentially constant for $t \geq 1.5$ h one might be misled into concluding that the AFC had ceased emitting antibodies. In fact, if complement were present in the media during the course of the experiment, one could not distinguish this case from that of a cell secreting antibodies at a constant rate forever.

Even though the three-dimensional result may be a valid approximation for over 50 h, eventually the two-dimensional result will be obeyed. This result clearly shows that the mathematical problem of

* The usual Einstein equation, in three dimensions, $\langle r^2 \rangle = 6Dt$ applies to an instantaneous source, $S(t) = S\delta(t)$. For a continuous source one finds $\langle r^2 \rangle = \int_0^\infty r^2 c(r, t) 4\pi r^2 \, dr/St = 3Dt$.

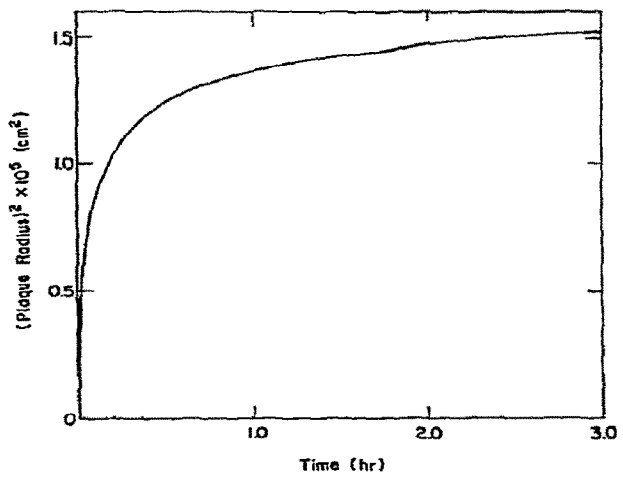

Fig. 5. The plaque radius squared as a function of time for an AFC in the center of a layer of thickness $h = 0.16$. The exact and infinite 3D results are indistinguishable for the times shown. The plaque radius is measured in the $z = 0$ plane. $\theta = 38$ and $D = 8.0 \times 10^{-8}$ cm^2/s.

plaque growth can fruitfully be interpreted as a multiple time scale problem and attacked from the viewpoint of perturbation theory.

4.3.3. The liquid layer

In the liquid layer assays the AFC fall to the bottom of the layer ($z' = -l$). Since the AFC are in contact with the boundary the infinite three-dimensional limit [eq. (9a)] can not hold, no matter how short the time. However, it is easy to modify the limit. At short times the upper boundary will have a negligible effect and therefore the limiting result is the solution to the problem of a source on top of an impenetrable surface where diffusion can take place anywhere above the surface. The solution of this problem is just the sum of the concentrations due to the source and its image. For a single boundary the source and image are equidistant from the plane (see fig. 2). As the source is moved closer to the boundary the image also moves closer. When the source is on the boundary so is the image. The effect of the boundary is to make the AFC appear to secrete at twice its true secretion rate. For an AFC on the boundary the short time limit is obtained by letting S equal $2S$ in eq. (9a), i.e.

$$2\pi DN/\upsilon KeS = (1/r_p)\,\mathrm{erfc}[(r_p^2/4D^*t)^{1/2}]. \qquad (34)$$

The long time limit, eq. (9b), remains unchanged.

The curve for the growth of a plaque produced by an AFC at the bottom of a liquid layer is shown in fig. 6. It can be seen that the semi-infinite three-dimensional result, obtained by solving eq. (34), agrees well with the exact result for $t \lesssim 5$ min.

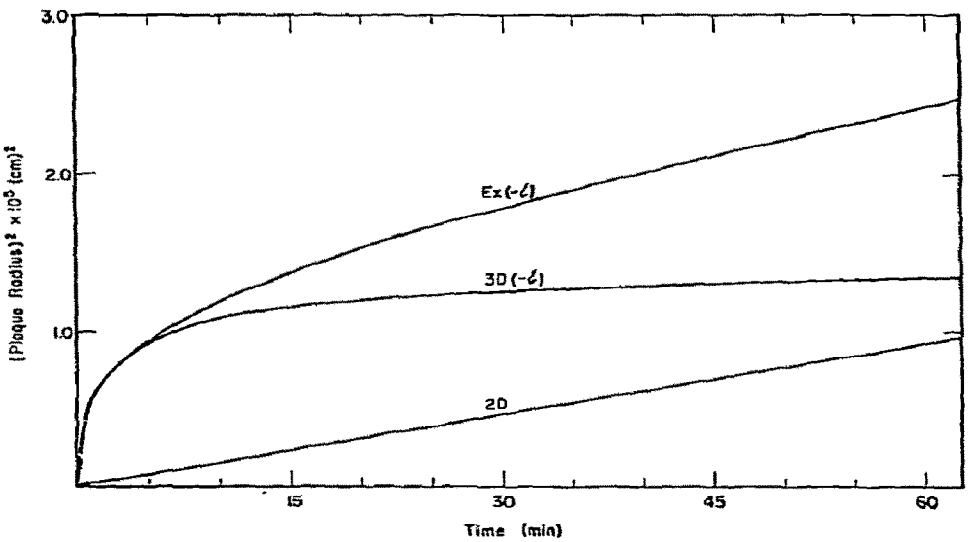

Fig. 6. The plaque radius squared as a function of time for an AFC at the bottom ($z = -l$) of a liquid layer ($D = 1.7 \times 10^{-7}$ cm^2/s) of thickness $h = 0.01$ cm. $\theta = 5.0$. Ex($-l$) and 3D($-l$) label curves corresponding to the exact and modified infinite three-dimensional results for the plaque radius measure at the bottom of the layer. 2D labels the curve for the two-dimensional limit.

4.4. Comparison with experiment

Merchant and Peterson [26] compared the distribution of plaque radii after 1 h obtained using a thin ($h = 3 \times 10^{-3}$ cm) microchamber technique with the distribution obtained using a thick layer ($h > 0.16$ cm) plaque-in-agar assay. For this microchamber assay eq. (28) predicts that the two-dimensional solution is valid when $t \gtrsim 40$ min, except possibly for the very weakest antibody secreters. For the thick gel eq. (33) predicts that the infinite three-dimensional result is valid, for all θ values of interest, for the entire duration of the experiment. Thus the limiting results can be used to analyze the experiments.

Given the distribution of plaque radii obtained in the microchamber one can predict the distribution in the thick gel. We have done this and in fig. 7 we compare our predictions with the experimental results. The theoretical distribution of plaque radii was obtained in the following way: the effective diffusion coefficient for IgM in the microchamber was taken to be $D_{20,w} = 1.7 \times 10^{-7}$ cm^2/s since no support material was used in the chamber. For each plaque radius $\beta = R_p^2/4D_{20,w}t$ was calculated for $t = 1$ h. Then the θ value corresponding to each R_p was obtained from eq. (27) and tables for the function $E_1(\cdot)$. The r_p values for the thick gel were then calculated from these θ values by using eq. (9a). D in the gel was taken to be 4.0×10^{-8} cm^2/s [29]. As one can see in fig. 7 the results are in good agreement, illustrating that the differences that Merchant and Peterson observed between the microchamber and plaque-in-agar techniques were mainly geometrical and due to the different values of D and h.

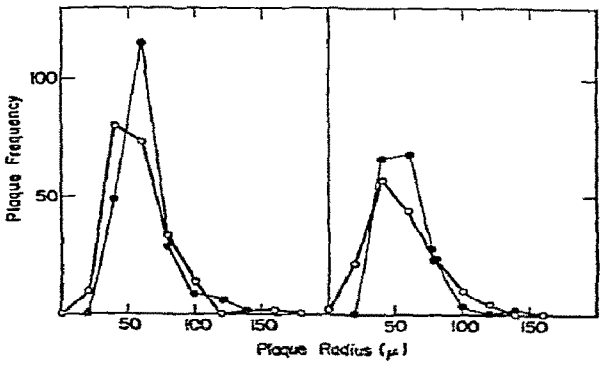

Fig. 7. The open circles (○) correspond to distributions of plaque radii as measured by Merchant and Peterson in a thick gel [26]. The results are reported for two mice. From distributions they obtained using a liquid microchamber (not shown) the expected distributions of plaque radii in thick gel have been calculated. The closed circles (●) are the theoretical predictions.

4.5. Applicability of the theory to the various assay systems

In various modifications of the plaque assay different geometries are used. Here we discuss the applicability of our results, which assume a single layer of thickness, h, to these systems.

Nossal et al. [25,27] use a plaque assay in which the layer containing the AFC, RBC, nutrient, support material and complement is plated directly on a slide and then covered with oil. Since there will be negligible diffusion of antibodies into the oil, the assay can be modeled as taking place in a layer bounded by two impenetrable surfaces. In some applications of the plaque-in-agar and liquid monolayer techniques there are two layers between the impenetrable surfaces which differ in that one contains RBC and AFC and the other does not. For example, this occurs in the plaque-in-agar technique when a bottom layer of agar is used. If D^*, the effective antibody diffusion coefficient in the layer containing the RBC, differs little from D_0, the antibody diffusion coefficient in the layer containing no cells, then one can calculate the free antibody concentration by considering a single layer whose thickness is the sum of the heights of the two layers. Of course, eq. (4) only holds in the layer which contains RBC since only in that layer can binding occur. We expect that for most direct plaque experiments it is reasonable to assume that $D^* \approx D_0$. Recall that $D^* = D/1(1 + \upsilon K \rho_0)$. The RBC cause D^* to differ from D_0 in two ways: they take up volume and therefore slow the diffusion of antibodies outward (if this is negligible then $D \approx D_0$); they bind antibodies and cause D^* to be reduced by $1/(1+\upsilon K \rho_0)$.

For typical plaque-in-agar assays the fraction of the volume taken up by RBC is small, of the order of a few percent [12,26]†. In a liquid microchamber ex-

† If the fraction of the volume occupied in a layer by RBC is $F = V_{RBC}/V_T$, where V_{RBC} is the RBC volume and V_T the total volume of the layer, then the change in D can be estimated from the formula $D = D_0(1-3F/2)$ [38]. (This result was derived for the conductivity of a layer with spheres of zero conductivity imbedded in it. This result holds for diffusion coefficients as well [39].) When $F = 0.02$, $D = 0.97$. For the liquid monolayer $F \approx 0.18$ and $D \approx 0.73\, D_0$.

periment the RBC can occupy a considerable fraction of the volume of the monolayer formed on the bottom of the chamber. (If the height of the monolayer is taken to be 7 μ, then in Merchant and Peterson's experiment [26], 18% of the volume of the monolayer is occupied by RBC.) However the volume of the monolayer is small compared to the total volume of the chamber (23% in ref. [26]) so that changes in the antibody concentration arise primarily from antibodies diffusing outside the monolayer with diffusion coefficient D_0. For this reason we feel the error introduced by assuming antibodies diffuse everywhere in the chamber with diffusion coefficient D_0 is small.

Usually, the effect of the binding is negligible on D^* for plaques formed by IgM through single site binding [3]. Typically for IgM binding to RBC $e \approx 10^5$ sites/RBC, $\rho_{RBC} \approx 2 \times 10^8$ RBC/cm^2, $\upsilon = 10$ and $K = 10^5$ M^{-1} so that $\upsilon K \rho_0 \approx 0.03$ and $D^* \approx 0.97\, D$. Thus we expect that the theory presented is applicable to the various assays discussed in section 2.

4.6. Choosing h for ease of interpretation of plaque experiments

When h is chosen such that either the two or infinite three-dimensional limiting cases hold, the mathematical expressions which describe plaque growth greatly simplify. This should be an important consideration for studies in which measurements of plaque radii are used to obtain quantitative information. However, even when only qualitative information is desired it may be important to choose h in a particular way. For example, if one is studying the effects of a metabolic poison where a decrease in secretion rate is expected then it is important not to use very thick layers. For in such layers the plaque will reach a steady state size, after which a decrease in secretion rate, even to zero, will have no effect on the plaque. This, of course, presumes that complement had been added to the layer at the beginning of the experiment so that the growth of the plaque could be followed in time. (The problems of determining variations in secretion rate by studying the time development of plaques in thin layers is discussed in ref. [9].)

The mathematical complexities of working with the two- and three-dimensional solutions are about equal, however, for certain types of studies one limit rather than the other may be particularly advantageous. If one is studying the effect of a parameter such as epitope density, antibody diffusion coefficient, or AFC secretion rate one would like to maximize the sensitivity of the plaque assay to changes in the parameter. If x is the parameter, then one wants to choose the two-dimensional limit if $dR_p/dx > dr_p/dx$ and choose the three-dimensional limit if $dr_p/dx > dR_p/dx$. For $x = S$ the secretion rate, one finds

$$\frac{d \ln r_p}{dx} = - \frac{1}{1 + h \exp(-\beta)/\theta (D^* t)^{1/2}} \frac{d \ln \theta}{dx}, \quad \text{three-dimensional;} \tag{35a}$$

$$d \ln R_p/dx = -\tfrac{1}{2} \exp(\beta)\theta \, d \ln \theta/dx, \quad \text{two-dimensional.} \tag{35b}$$

As $t \to \infty$ eq. (35a) simplifies to

$$d \ln r_p/dx = - d \ln \theta/dx. \tag{36}$$

Thus when $\frac{1}{2}\exp(\beta)\theta = \frac{1}{2}\exp(\beta)E_1(\beta)$ is greater than 1, the fractional change in the two-dimensional plaque radius, R_p, is greater than the fractional change in the steady state three-dimensional plaque radius, r_p, for equal variation of the secretion rate. Since $\frac{1}{2}\exp(\beta)E_1(\beta) > 1$ for $\beta < 0.1$ or $\theta = E_1(\beta) > 1.8$ one should use a thin layer system to study AFC with $\theta > 1.8$ (weak antibody secreters) and thick layer systems to study AFC with $\theta < 1.8$ (strong antibody secreters). A similar analysis can be done for other choices of the varied parameter x.

In some instances it may be useful to have a plaque reach a final steady state size. In such circumstances a thick layer system should be used. The time it takes a plaque to reach, say 95% of steady state size may be estimated as follows:

$$r_p/r_p(t \to \infty) = \operatorname{erfc}(\beta^{1/2}).$$

Let m be such that $\operatorname{erfc}(m) = 0.95$; i.e. $m = 0.056$; then $m^2 = \beta = r_p^2/4D^* t_{0.95}$ or

$$t_{0.95} = (0.95)^2 h^2/4\theta^2 m^2 D^* = 71.9\, h^2/\theta^2 D^*, \tag{37}$$

where we have replaced r_p by $0.95 r_p(t \to \infty)$ and we have replaced $r_p(t \to \infty)$ by h/θ.

4.7. Multisite binding

If on the RBC surface the density of binding sites

is high enough then a single antibody can bind more than one RBC binding site. Such multisite attachments have been modeled as an irreversible reaction for $t \lesssim 1$ h [7]. For such binding, the growth of plaques has been studied in the two limiting cases of two-dimensional and infinite three-dimensional diffusion [7,8]. Results similar to those represented by eq. (24) can be obtained for the finite layer geometry by using the same techniques as outlined in section 3. For completeness the multisite results are summarized in appendix 2.

5. Summary

The kinetics of hemolytic plaque growth is determined in part by the thickness of the layer used in the assay. For the range of layer thicknesses commonly used, the time development can vary dramatically. At one extreme is the thin layer (or long time limit) where the diffusion is planar [two-dimensional limit, eq. (9b)]. At the other extreme is the thick layer (or short time limit) where the diffusion is unaffected by the boundaries [infinite three-dimensional limit, eq. (9a)]. When the binding of antibodies to RBC is equilibrium controlled, and the AFC secrete antibodies at a constant rate, R_p^2/t = constant in the two-dimensional limit, while in the infinite three-dimensional limit, the plaque radius starts out growing rapidly and then approaches a constant value. For typical plaque experiments ($t \approx 1$ h) the two-dimensional limit will hold for layer thicknesses $h \lesssim 3.0 \times 10^{-3}$ cm, while the infinite three-dimensional limit will hold for $h \gtrsim 10^{-1}$ cm. An exception to the latter case is when an AFC is near the top or bottom of the layer. Then deviations from the infinite three-dimensional limit can occur for $t < 1$ h. In the liquid layer techniques the AFC are on the bottom of the layer. The effect of the boundary is to cause twice as many antibodies to diffuse into the upper half plane (above the AFC) as would if no boundary were present. The AFC thus, at short times, appears to secrete antibodies at twice its true secretion rate. The thick layer (or short time) limit for the liquid layer, eq. (34), is obtained by replacing S by $2S$ in the equation for the infinite three-dimensional limit [eq. (9a)].

When $3.0 \times 10^{-3} < h < 1.0 \times 10^{-1}$, for at least some AFC, neither limiting result will give the correct description of plaque growth. Then one must use the more complicated exact results, eq. (24), to predict the proper time development of the plaque. It is exceedingly important to know the value of h in order to properly interpret plaque data. If the wrong limit is applied, one can be grossly misled about the behavior of the AFC.

Appendix 1

We derive a necessary condition for the validity of the infinite three-dimensional solution when θ takes on large values. We consider only the case when the AFC is in the center of the gel. The exact equation, eq. (24a), reduces to the three-dimensional limit when σ_3 can be approximated by its first term, i.e.

$$(h/r)\,\mathrm{erfc}[(r^2/4D^*t)^{1/2}] \gg h \sum_{\substack{n=-\infty \\ n\neq 0}}^{\infty} \mathrm{erfc}[(d_n^2/4D^*t)^{1/2}]/d_n \qquad (1.1)$$

[see eq. (19)].

The plaque radius is closest to the boundary on the z-axis. At the point $(0,0,z_p)$, eq. (1.1) becomes

$$(1/f)\,\mathrm{erfc}\,(fB_0^{1/2}) \gg \sum_{n=1}^{\infty} \frac{1}{n}\left[\frac{\mathrm{erfc}[n(1-f/n)B_0^{1/2}]}{1-f/n} + \frac{\mathrm{erfc}[n(1+f/n)B_0^{1/2}]}{1+f/n}\right], \qquad (1.2)$$

where $f = z_p/h$ and $B_0^{1/2} = h^2/4D^*t$. When the three-dimensional solution holds

$$\theta = (1/f)\,\mathrm{erfc}\,(fB_0^{1/2}). \qquad (1.3)$$

Since $1 \geqslant \mathrm{erfc}\,(x)$ for x, $f < 1/\theta$. For large θ, $f/n \ll 1$. Neglecting terms of order f/n eq. (1.2) becomes

$$(1/f)\,\mathrm{erfc}\,(fB_0^{1/2}) \gg 2\sum_{n=0}^{\infty} (1/n)\,\mathrm{erfc}\,(nB_0^{1/2}). \qquad (1.4)$$

We assume that for $n > n^*$, the argument of erfc ($\cdot$) is such that the higher terms in the sum can be neglected. This value of the argument we call c [in numerical work we take $c = 1.16$, i.e., $\mathrm{erfc}\,(c) = 0.1$]

$$n^* B_0^{1/2} = c. \qquad (1.5)$$

We define t_3 so that at $t = t_3$ eq. (1.5) is satisfied.

Thus

$$t_3 = (n^*)^2 h^2 / 4D^* c^2. \tag{1.6}$$

For $t \leqslant t_3$ eq. (1.4) now becomes

$$(1/f)\,\mathrm{erfc}\,(fB_0^{1/2}) \gg 2S(n^*), \tag{1.7}$$

where

$$S(n^*) = \sum_{n=1}^{n^*} (1/n)\,\mathrm{erfc}\,(nc/n^*). \tag{1.8}$$

When the three-dimensional solution holds the right hand side of eq. (1.7) equals θ, i.e.

$$\theta \gg 2S(n^*). \tag{1.9}$$

In table 4 we list values of $S(n^*)$ for various n^*. To each value of n^* there corresponds by eq. (1.6) a value of t_3. Thus for all $\theta \gg 2S(n^*)$, it is necessary for t to be less than t_3 for the three-dimensional solution to hold. We assume eq. (1.9) holds when $\theta \geqslant \theta_{\min} = 200S(n^*)$.

Appendix 2

The time development of a plaque produced by an AFC in a finite layer depends both on the thickness of the layer and the way in which antibodies bind to RBC. In the text we treated a particular binding scheme, that where the free and bound antibodies are in local equilibrium. However, the method we used is quite general and can be applied to a variety of antibody–RBC interactions. Here we outline how to obtain solutions when (1) the antibodies bind irreversibly to the RBC surface ($k_r = 0$) and (2) the fraction of sites bound on any RBC is small ($\rho \approx \rho_0$). With these conditions c_b obeys the following equation:

$$\partial c_b/\partial t = v k_f c \rho_0 \tag{2.1}$$

and the equation to be solved is therefore

$$(1/D)\,\partial c/\partial t = \nabla^2 c - (v/D) k_f \rho_0 c + (S/D)\delta(x)\delta(y)\delta(z - z'), \tag{2.2}$$

where at $z = \pm l$, $\partial c/\partial z = 0$, and $c(x, y, z, t) \to 0$ as $x, y \to \infty$ for all finite t.

We follow the procedure outlined in section 3 and first solve for $c' = \partial c/\partial t$ and then integrate c' over time to obtain c. The equation for c' can be obtained from eq. (2.2) by replacing S by $S\delta(t)$. For the case of an infinite three-dimensional geometry [8],

$$c'(r, t) = S(4\pi Dt)^{-3/2} \exp(-D\lambda^2 t - r^2/4Dt), \tag{2.3}$$

where $\lambda = (v k_f \rho_0 / D)^{1/2}$.

The solution to the finite layer problem is obtained by adding up all the contributions from the image sources. The result is just eq. (16) with $D^* = D$ and $\exp(-D\lambda^2 t)$ multiplying the entire expression. When $c'(x, y, z, \tau)$ is integrated over τ from 0 to t, the result is:

$$c(x, y, z, t) = (S/8\pi Dh)\sigma_3, \tag{2.4}$$

where

$$\sigma_3 = h \sum_{n=-\infty}^{\infty} [\exp(-\lambda r_n)\,\mathrm{erfc}[\beta_n^{1/2} - \lambda(Dt)^{1/2}]/r_n + \exp(\lambda r_n)\,\mathrm{erfc}[\beta_n^{1/2} + \lambda(Dt)^{1/2}]/r_n + \exp(-\lambda L_n)\,\mathrm{erfc}[B_n^{1/2} - \lambda(Dt)^{1/2}]/L_n + \exp(\lambda L_n)\,\mathrm{erfc}[B_n^{1/2} + \lambda(Dt)^{1/2}]/L_n]. \tag{2.5}$$

The parameters β_n, B_n, r_n and L_n are defined by eqs. (18b)–(18e) with $D^* = D$.

Eq. (2.3) converges rapidly for short times. To ob-

Table 4 [a]

n^*	$S(n^*)$	$\theta_{\min}$	$t_3(h = 5 \times 10^{-2}$ cm) (h)
1	0.101	20.2	0.76
2	0.463	92.6	3.04
3	0.755	151.0	6.83
4	0.986	197.2	12.14
5	1.175	235.0	18.97
6	1.334	266.8	27.32
7	1.471	294.2	37.19
8	1.593	318.6	48.57
9	1.701	340.2	61.47
10	1.798	359.6	75.89

[a] $S(n^*) = \Sigma_{n=1}^{n^*} (1/n)\,\mathrm{erfc}\,(nc/n^*)$, where $c = 1.16$. $\theta_{\min}$ is the minimum value of θ for which $\theta \geqslant 200\,S(n^*)$. t_3 has been calculated for a layer of thickness $h = 5 \times 10^{-2}$ cm and $D = 1.7 \times 10^{-7}$ cm^2/s. For a given θ, it is necessary for t to be less than t_3 for the three-dimensional solution to hold. For the largest estimate of t_3 choose the t_3 value corresponding to the largest value of $\theta_{\min}$ for which $\theta > \theta_{\min}$.

tain a series that converges rapidly for long times just as in the text, one transforms c' with eq. (19) and then integrates.

Appendix 3: List of symbols

AFC = antibody forming cell.
c = free antibody concentration.
c' = $\partial c/\partial t$.
c_b = bound antibody concentration.
D = diffusion coefficient of an antibody in the layer in the presence of RBC.
D_0 = diffusion coefficient of an antibody in the layer in the absence of RBC.
$D_{20,w}$ = diffusion coefficient of an antibody in water at a temperature of 20°C.
D^* = the hindered diffusion coefficient equal to $D/(1+\upsilon K\rho_0)$.
e = epitope density, i.e. the number of binding sites per RBC.
f = r_p/h^*.
h = the total thickness of the layer.
h^* = the distance from the AFC to its nearest image.
k_f = overall forward rate constant for the binding of an antibody combining site with the RBC surface.
k_r = overall reverse rate constant for the dissociation of an antibody combining site with the RBC surface.
K = k_f/k_r, affinity of a single antibody combining site with the RBC surface.
l = half thickness of the layer ($l = h/2$).
N = average number of antibodies bound to a RBC at the plaque radius.
r = three-dimensional position vector.
R = two-dimensional position vector.
r_p = plaque radius in the infinite three-dimensional limit when the plaque is spherical.
R_p = plaque radius in the two-dimensional limit when the plaque is cylindrical.
RBC = red blood cells.
S = rate (Ab/s) at which antibodies are secreted by the AFC.
t = secretion time equal to $T-T_0$.
T = total time the AFC is in the layer.
T_0 = the time at which the AFC starts secreting.
t_2 = time beyond which the two-dimensional result holds.
t_3 = time up to which the three-dimensional result holds.
z' = position of the AFC above the center of the layer.
β = $R_p^2/4D^*t$.
θ = $4\pi DhN/\upsilon KeS$, a parameter that characterizes the the strength of the AFC.
ρ = concentration of free antigenic determinants (free RBC binding sites).
ρ_0 = total (free plus bound) concentration of binding sites.
ρ_{RBC} = concentration of RBC.
σ_2 = infinite sum which converges to the two-dimentional limit at long times.
σ_3 = infinite sum which converges to the three-dimensional limit at short times.

References

[1] G.M. Edelman and J.A. Gally, J. Exp. Med. 116 (1962) 207.
[2] N.K. Jerne and A.A. Nordin, Science 140 (1963) 405.
[3] A.S. Perelson and B. Goldstein, J. Immunol., to be published.
[4] J.M. Jones, D.F. Amsbaugh and B. Prescott, J. Immunol. 116 (1976) 52.
[5] B. Anderson, J. Exp. Med. 132 (1970) 77.
[6] B. Goldstein and A.S. Perelson, Biophys. Chem. 4 (1976) 349.
[7] C.P. DeLisi and G.I. Bell, Proc. Natl. Acad. Sci. US 71 (1974) 16.
[8] C.P. DeLisi, J. Math. Biol. 2 (1975) 317.
[9] B. Goldstein, in: Theoretical immunology, eds. G.I. Bell, A.S. Perelson and G.H. Pimbley (Dekker, New York) to be published.
[10] N.K. Jerne, A.A. Nordin and C. Henry, in: Cell-bound antibodies, eds. B. Amos and H. Koprowski (Wistar Institute Press, Philadephia, 1963) p. 109.
[11] J.H. Humphrey, Nature 216 (1967) 1295.
[12] N.K. Jerne, C. Henry, A.A. Nordin, H. Fuji, A.M.C. Koros and I. Lefkovits, Transplant. Rev. 18 (1974) 130.
[13] B. Merchant and T. Hraba, Science 152 (1966) 1378.
[14] M.N. Layson and A.H. Sehon, Can. J. Biochem. 45 (1967) 1773.
[15] P. Walsh, P. Maurer and M. Egan, J. Immunol. 98 (1967) 344.
[16] E.S. Golub, R.I. Mishell, W.O. Weigle and R.W. Dutton, J. Immunol. 100 (1968) 133.
[17] D.W. Dresser and H.H. Wortis, Nature 208 (1965) 859.
[18] J. Sterzl and I. Riha, Nature 208 (1965) 858.
[19] E. Weiler, E.W. Melletz and E. Breuninger-Peck, Proc. Natl. Acad. Sci. US 54 (1965) 1310.

[20] J.S. Ingraham and A. Bussard, J. Exp. Med. 119 (1964) 667.
[21] A.J. Cunningham, Nature 207 (1968) 1106.
[22] A.J. Cunningham and A. Szenberg, Immunol. 14 (1968) 599.
[23] M.A. Axelrod and J.C. Kennedy, Immunol. 20 (1971) 253.
[24] J.S. Ingraham, A.A. Biegel, M.R. Watanabe and C.W. Todd, J. Immunol. 99 (1967) 1023.
[25] G.J.V. Nossal, A.E. Bussard, H. Lewis and J.C. Mazie, J. Exp. Med. 131 (1970) 894.
[26] B. Merchant and B. Peterson, J. Immunol. 110 (1968) 860.
[27] B. Merchant, private communication.
[28] A.J. Cunningham and S.A. Fordham, Nature 250 (1974) 669.
[29] G.J.V. Nossal and H. Lewis, Immunol. 20 (1971) 739.
[30] C.L. Hornick and F. Karush, Immunochem. 9 (1972) 325.
[31] B. Goldstein, C. DeLisi and J. Abate, J. Theor. Biol. 52 (1975) 317.
[32] W.R. Smythe, Static and dynamic electricity, 3rd Ed. (McGraw-Hill, New York, 1950).
[33] H.S. Carslaw and J.C. Jaeger, Conduction of heat in solids, 2nd Ed. (Oxford Univ. Press, London, 1959).
[34] M. Abramowitz and I.A. Stegun, eds., Handbook of mathematical functions (National Bureau of Standards, Washington, 1964).
[35] T.J. Dekker, in: Constructive aspects of the fundamental theorem of algebra, eds. B. Dejon and P. Henrici (Wiley, New York, 1969).
[36] E.A. Kabat and K.O. Pederson, Science 87 (1938) 372.
[37] T. Suzuki and H.F. Deutsch, J. Biol. Chem. 242 (1967) 2725.
[38] R. Landauer, J. Appl. Phys. 23 (1952) 779.
[39] I. Fatt and R.C. LaForce, J. Phys. Chem. 67 (1963) 2260.